The Griffiths phase and beyond: A large deviations study of the magnetic susceptibility of the two-dimensional bond-diluted Ising model

L. Münster,[1] A. K. Hartmann,[2] and M. Weigel[1]

[1] *Institut für Physik, Technische Universität Chemnitz, 09107 Chemnitz, Germany*
[2] *Institut für Physik, Universität Oldenburg, 26111 Oldenburg, Germany*

(Dated: August 29, 2024)

The Griffiths phase in systems with quenched disorder occurs below the ordering transition of the pure system down to the ordering transition of the actual disordered system. While it does not exhibit long-range order, large fluctuations in the disorder degrees of freedom result in exponentially rare, long-range ordered states and hence the occurrence of broad distributions in response functions. Inside the Griffiths phase of the two-dimensional bond-diluted Ising model the distribution of the magnetic susceptibility is expected to have such a broad, exponential tail. A large-deviations Monte Carlo algorithm is used to sample this distribution and the exponential tail is extracted over a wide range of the support down to very small probabilities of the order of 10^{-300}. We study the behavior of the susceptibility distribution across the full phase diagram, from the paramagnetic state through the Griffiths phase to the ferromagnetically ordered system and down to the zero-temperature point. We extract the rate function of large-deviation theory as well as its finite-size scaling behavior and we reveal interesting differences and similarities between the cases. A connection between the fraction of ferromagnetic bonds in a given disorder sample and the size of the magnetic susceptibility is demonstrated numerically.

PACS numbers: 05.10.Ln,75.10.Hk,75.50.Lk

I. INTRODUCTION

The Ising model is one of the most studied systems in statistical physics and has found applications in many branches of science, see, e.g., Refs. [1–6]. Its original purpose is to describe ferromagnetism in homogeneous materials with strong uniaxial asymmetry. Often, however, materials are not perfectly homogeneous but exhibit randomly distributed impurities. In such cases, a central question is how these random impurities affect the physical properties of the system in comparison to the idealized pure model [7]. Impurities can be incorporated into the Ising model, for instance, by randomly removing a fraction $1 - p$ of the bonds that represent the ferromagnetic interactions between the spins, where $0 \leq p \leq 1$. Due to the overall weakened ferromagnetic coupling this leads to a shift in the transition temperature from $T_\mathrm{f} := T_\mathrm{c}(p = 1)$ in the pure system to a lower temperature $T_\mathrm{c}(p),\ p < 1$ in the diluted system. As shown by Harris [8], the critical behavior at the transition differs from that found in the pure system if the specific heat exponent α of the pure system is positive. This is the case for the Ising model in dimensions $d \geq 3$, while $\alpha = 0$ in $d = 2$. Due to this marginality one expects logarithmic corrections to the leading critical behavior in two dimensions, but according to numerical simulations [9–11] as well as experiments [12, 13] the critical exponents remain identical to the pure case.

The thermal region between T_f and $T_\mathrm{c}(p < 1)$ is known as the *Griffiths phase* [14]. In this regime the order parameter of the ferromagnetic phase transition, the magnetization, remains zero, But arbitrarily large fluctuations of the order parameter become possible. These fluctuations can exist due to large compact structures of ferromagnetic bonds in regions where there are less missing bonds in comparison to the overall average of the system. Within these structures the system is effectively in a ferromagnetic state such that a change of the spin orientation happens coherently, giving rise to large fluctuations in the magnetization. As a consequence the distribution of the second moment of the magnetization, the magnetic susceptibility, is expected to have an exponential tail that extends to infinity, which is an expression of the essential, but weak, Griffiths singularity [15, 16]: Since the magnetic susceptibility characterizes the response of the system to an external magnetic field, the free energy is a non-analytic function of the field throughout the Griffiths phase [14]. Besides these effects on static averages, the Griffiths singularity also plays an important role for the dynamics of the system, leading to a slow-down of the decay of the spin-spin correlation function [15, 17, 18]. The Griffiths singularity does not only occur in the diluted Ising ferromagnet [19] but it may also be observed in other disordered systems such as spin glasses [20]. The analogous quantum mechanical effect is known as the Griffiths-McCoy singularity, and it has been studied theoretically, numerically as well as in experiments [21–27].

In the present work we use numerical simulations [28] using the Monte Carlo approach [29] to explore the Griffiths phase by investigating the distribution over the bond disorder of the magnetic susceptibility in the two-dimensional bond-diluted Ising ferromagnet. In particular, we are interested in the tail of the distribution. To obtain this tail we employ a large-deviation sampling algorithm [30] which has previously proved useful for a variety of rare-event sampling problems. A drawback of the variant of the algorithm used to date is that for

some cases it does not scale well with increasing system size [31]. For the system at hand, we resolve this problem by using a different bias for the sampling process, see Sec. III for details. The authors of a previous study of the bond-diluted Ising model [32] performed a similar analysis of the magnetic susceptibility, but they were only able to sample relatively closely to the mean value of the distribution. Here, the distribution will be presented over a wide range of its support. Furthermore, the distribution of the magnetic susceptibility is also studied at the critical temperature and inside the ferromagnetic phase. Interestingly, an exponential tail is also found for the distribution inside the ferromagnetic phase but the mechanism leading to it appears to be different from that in the Griffiths phase.

The rest of this paper is organized as follows. In Sec. II we introduce the two-dimensional bond-diluted Ising model and discuss its essential properties in so far as they are relevant in the context of the present study. In Sec. III the large-deviation sampling algorithm of Ref. [30] is summarized and we introduce a weight-construction scheme based on ideas of Neuhaus and Hager [33]. In Sec. IV we present our simulation results for the disorder distribution of the magnetic susceptibility inside the Griffiths phase and at the critical temperature, while Sec. V is devoted to our results for the distribution inside the ferromagnetic phase and at zero temperature. Finally, Sec. VI contains a discussion and outlook.

II. THE TWO-DIMENSIONAL BOND-DILUTED ISING FERROMAGNET

The Hamiltonian of the bond-diluted Ising ferromagnet is given by

$$\hat{H}_{\boldsymbol{J}}\left(\boldsymbol{S}\right) = -\sum_{\langle \boldsymbol{x},\boldsymbol{y}\rangle} J_{\boldsymbol{xy}} s_{\boldsymbol{x}} s_{\boldsymbol{y}} - h\hat{M}, \tag{1}$$

where $\boldsymbol{S} \in \{-1,1\}^N$ denotes a spin configuration, and $\hat{M} = \sum_{\boldsymbol{x}} s_{\boldsymbol{x}}$ represents the configurational magnetization which couples to the external magnetic field h. The Ising spins $s_{\boldsymbol{x}} = \pm 1$ are placed at the sites $\boldsymbol{x}$ of a two-dimensional square lattice of linear dimension L, resulting in $N = L^2$ spins in total. The notation $\langle \boldsymbol{x}, \boldsymbol{y}\rangle$ refers to summation over nearest neighbors only. The time-independent, quenched interaction between two spins is represented by the exchange coupling $J_{\boldsymbol{xy}}$. To incorporate random dilution into the model, the bonds are drawn from a bimodal distribution, such that the probability to obtain a particular bond sample $\boldsymbol{J} = \{J_{\boldsymbol{xy}}\}$ is given by

$$P_J(\boldsymbol{J}) = \prod_{\langle \boldsymbol{x},\boldsymbol{y}\rangle} p\,\delta[J_{\boldsymbol{xy}} - 1] + (1-p)\delta[J_{\boldsymbol{xy}}]. \tag{2}$$

where we use $\delta[x]$, $x \in \mathbb{R}$, as an indicator function that yields one if $x = 0$ and zero otherwise. Here, p corresponds to the probability of drawing a ferromagnetic bond with $J_{\boldsymbol{xy}} = 1$, while $1-p$ is the probability of missing bonds with $J_{\boldsymbol{xy}} = 0$. The model is studied in the canonical ensemble at temperature T, such that the spin configurations $\boldsymbol{S}$ are Boltzmann distributed according to

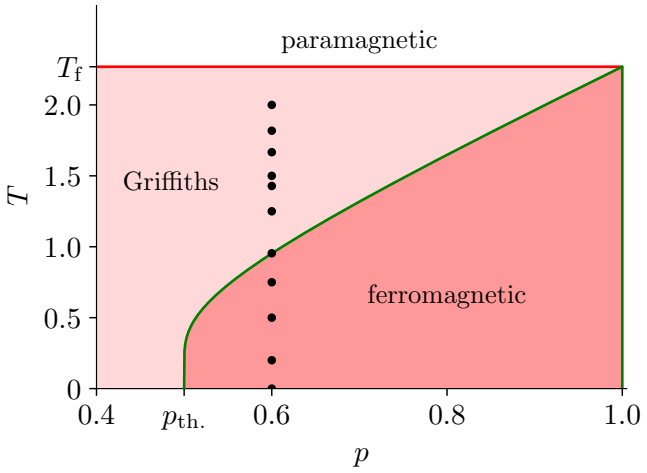

FIG. 1. Zero-field phase diagram of the two-dimensional bond-diluted Ising ferromagnet as a function of the fraction p of ferromagnetic bonds and the temperature T. The boundary between the ferromagnetic and paramagnetic phase is obtained according to the "$s = 1$" technique of Ohzeki [34]. The black dots at $p = 0.6$ mark the temperatures at which our simulations are performed.

$$P_S(\boldsymbol{S}|\boldsymbol{J}) = \frac{1}{Z_{\boldsymbol{J}}} \exp\left\{-\hat{H}_{\boldsymbol{J}}(\boldsymbol{S})/T\right\}, \tag{3}$$

where we have set the Boltzmann constant $k_{\mathrm{B}} := 1$ for convenience. $Z_{\boldsymbol{J}}$ is the partition function for a given bond sample $\boldsymbol{J}$. The Gibbs state of the model in the absence of an external magnetic field, $h = 0$, depends on two parameters, the bond occupation probability p and the temperature T. The order parameter which can be used to determine the phase of the Gibbs state is the first moment of the magnetization per site [35]

$$\overline{m} = \left[\langle \hat{m} \rangle_S\right]_J, \tag{4}$$

where $\hat{m} = \hat{M}/N$. Here, $\langle\cdot\rangle_S$ denotes the thermal average with respect to the Boltzmann distribution, Eq. (3), and $[\cdot]_J$ is the average with respect to the disorder distribution, Eq. (2). As is clear from the phase diagram of the system shown in Fig. 1, there exists a high temperature paramagnetic phase and a low temperature ferromagnetic phase. The boundary between these phases extends from the bond-percolation threshold $p_{\mathrm{th}} = 0.5$ at which the transition temperature is zero, $T_{\mathrm{c}}(0.5) = 0$, to that of the pure ferromagnet with $p = 1$ and $T_{\mathrm{f}} = T_{\mathrm{c}}(1) = 2/\ln(1+\sqrt{2}) = 2.2691\ldots$. In between these limits, the phase boundary can be obtained by arguments based on duality [34, 36] which yield a good estimate for the true curve, consistent with what is found in numerical simulations [37]. The thermal region between

	$\Theta_k,\ k=1,\ldots,11$										
k	1	2	3	4	5	6	7	8	9	10	11
θ_1	-3	0	0.9	1	1	1	1	1	1	1.5	3
$1/\theta_2$	0	0	0	5	5	5	5	5	5	0	0
θ_3	0	0	0	10	20	30	40	50	60	0	0

TABLE I. Simulation parameters used to generate the histogram data shown in Fig. 2(b). There are eleven parameter sets in total, $\Theta_k,\ k=1,\ldots,11$. The parameter set $k=2$ corresponds to unbiased sampling. For $k=3$ the Monte Carlo process oscillates between small and large values.

the ferromagnetic phase transition of the pure system at $T_\mathrm{f}=T_\mathrm{c}(1)$ and the ferromagnetic phase transition in the diluted system $T_\mathrm{c}(p<1)$ is known as the Griffiths phase. Inside the Griffiths phase the order parameter remains zero but large fluctuations of the magnetization are more likely than in the paramagnetic phase. These fluctuations are visible in the magnetic susceptibility $\chi_{\boldsymbol{J}}$ which can be defined from the variance of the magnetization per lattice site for a given bond sample $\boldsymbol{J}$,

$$\chi_{\boldsymbol{J}} = N\left(\langle \hat{m}^2\rangle_S - \langle \hat{m}\rangle_S^2\right), \tag{5}$$

where $\langle \hat{m}\rangle_S = 0$ if $T \geq T_\mathrm{c}$. Bray [15] has predicted that the probability distribution of the magnetic susceptibility over the bond samples displays an exponential tail throughout the Griffiths phase. The functional form of this tail was derived to follow the form [15]

$$P_\chi(\chi) \sim \exp\left(-A\chi - 2\ln\chi\right) \tag{6}$$

for $\chi\to\infty$. Here, A is a temperature-dependent positive constant which vanishes at the ferromagnetic phase transition (implying a particularly broad distribution there) and diverges when T approaches T_f (such that the tail disappears in the non-disordered limit). Since the derivation which leads to Eq. (6) includes variational arguments and a number of approximations, Bray concluded that this form may only constitute a lower bound for the true tail. The magnetic susceptibility describes the linear response of the magnetization to an external magnetic field, since $(\partial/\partial h)\langle \hat{m}\rangle_S = \chi_{\boldsymbol{J}}/T$. Correspondingly, inside the Griffiths phase the free energy is a non-analytic function of the external magnetic field [14].

The origin of the large values of the magnetic susceptibility inside the Griffiths phase are compact structures of ferromagnetic bonds. In these local structures the fraction of ferromagnetic bonds is larger than the average expected fraction p of the infinite system. Below the ferromagnetic phase transition, i.e., for $T<T_\mathrm{c}(p<1)$, there also can be large fluctuations in the magnetization, but these are caused by a different mechanism which we will explore below. In both cases, bond samples which lead to larger than average values of the magnetic susceptibility occur rather rarely. Therefore, to numerically investigate the disorder distribution of the magnetic susceptibility it is necessary to employ large-deviation sampling techniques. These are the subject of the next section.

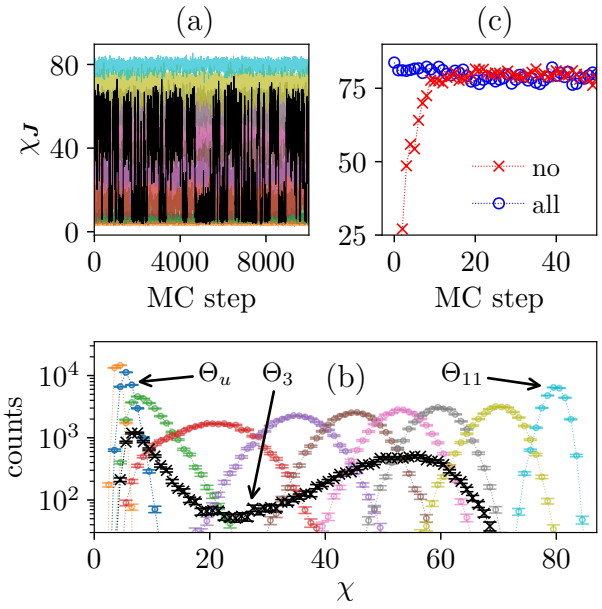

FIG. 2. **COMMENT Alex**: *Irgendwie sind die Figures recht weit weg von der ersten Erwähnung, man muss immer weit zurück blättern, bitte verschieben ...* Sampling procedure of the large-deviation algorithm to sample the magnetic susceptibility of the two-dimensional bond-diluted Ising ferromagnet at $T=2$ with $L=10$ and $p=0.6$. (a) Estimates of $Y_{\boldsymbol{J}}=\chi_{\boldsymbol{J}}$ in the bond Monte Carlo chain generated by the biased bond distribution, see Eq. (8), for various sets of parameters. (b) Histograms of sampled observable values in the different biased ensembles after a binning of the data from the different Monte Carlo chains. The corresponding parameters are listed in Table I. The unbiased distribution corresponds to $\Theta_u=\Theta_2=(0,0,0)$. The set $\Theta_3=(0.9,0,0)$ is special because in this case the observable oscillates between small and large values. The corresponding data in (a) and (b) is colored black. (c) Equilibration phase of a Monte Carlo process for $\Theta_{11}=(3,0,0)$. The Monte Carlo chains are initialized with no bonds or all bonds present, respectively. After approximately 20 Monte Carlo steps both chains start to oscillate around the same value indicating that equilibrium has been reached.

III. LARGE DEVIATIONS SAMPLING

To sample the distribution of the magnetic susceptibility over a wide range of the support we use the large-deviation Monte Carlo algorithm proposed in Ref. [30]. The basic idea of this method is to utilize an auxiliary Markov chain Monte Carlo process in the disorder degrees of freedom that is biased in such a way that it creates bond configurations that lead to the desired values in a quantity of interest such as, in our case, the susceptibility. The bias is then removed *a posteriori* by reweighting, such that at the end the thermodynamically correct distribution is obtained.

To be more specific, assume that the disorder dependent quantity of interest is $Y_{\boldsymbol{J}}$, where in our particular

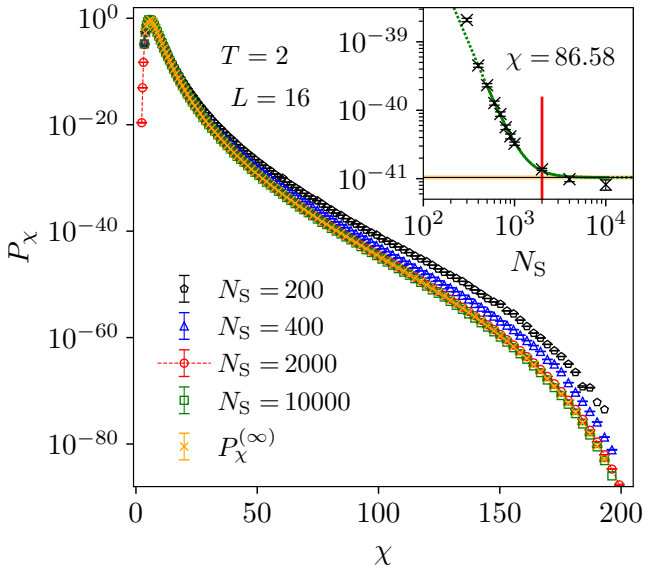

FIG. 3. Distribution of the magnetic susceptibility at $T = 2$ inside the Griffiths phase for $L = 16$. The plot illustrates how the measured distribution depends on the number N_S of samples used to compute the estimate of the observable $\chi_{\boldsymbol{J}}$. The extrapolated curve is obtained by a power-law fit $P_\chi(\chi; N_S) = c_1(\chi) N_S^{-c_2(\chi)} + P_\chi^{(\infty)}(\chi)$ at each bin, where c_1 and c_2 are fit parameters. The inset shows the power-law fit for the bin at $\chi = 86.58$. The green line corresponds to the fit, and its solid part indicates the fit range. The orange shaded area has a width of two times the standard error with the value of $P_\chi^{(\infty)}$ at its center. The red vertical line in the inset marks $N_S = 2000$, the number of samples that is used throughout the rest of this work.

case $Y_{\boldsymbol{J}} = \chi_{\boldsymbol{J}}$ and thus $Y_{\boldsymbol{J}} \geq 0$ [38]. The probability distribution of this quantity can be written as

$$P_Y(Y) = \sum_{\boldsymbol{J}} P_J(\boldsymbol{J}) \delta[Y_{\boldsymbol{J}} - Y] \tag{7}$$

where $P_J(\boldsymbol{J})$ is the unbiased bond distribution as given in Eq. (2). If we draw bonds from the unbiased distribution, this will only give us the typical values of $Y_{\boldsymbol{J}}$ in the region where the distribution $P_Y(Y)$ has most of its weight. To receive bond samples which lead to $Y_{\boldsymbol{J}}$ in the range of interest, i.e., where $P_Y(Y)$ is extremely small, we introduce a Monte Carlo process that generates samples from a biased bond distribution,

$$\widetilde{P}_J(\boldsymbol{J}; \Theta) = \frac{P_J(\boldsymbol{J}) f_\Theta(Y_{\boldsymbol{J}})}{Z_\Theta}. \tag{8}$$

Here, Z_Θ is a normalization constant that will be determined later, and $f_\Theta(Y_{\boldsymbol{J}})$ is a bias function which depends on the set of parameters Θ. The bias function has to be chosen such that $\widetilde{P}_J(\boldsymbol{J}; \Theta)$ defines a distribution which has enough weight in the regions that one would like to sample. Following the proposal of Neuhaus and Hager in Ref. [33] for a related problem, we conjecture that in many cases a generalized exponential of the form

$$f_\Theta(Y_{\boldsymbol{J}}) = \exp\left\{\theta_1 Y_{\boldsymbol{J}} - \frac{\theta_2^2}{2}(Y_{\boldsymbol{J}} - \theta_3)^2\right\} \tag{9}$$

with $\Theta = (\theta_1, \theta_2, \theta_3) \in \mathbb{R}^3$ serves this purpose well. To explain the effect of parameter θ_1, we first set $\theta_2 = 0$ such that f_Θ becomes a simple exponential. Now, if $\theta_1 < 0$ the weight of the bond samples with small $Y_{\boldsymbol{J}}$ in comparison to typical values of the unbiased distribution increases, and if $\theta_1 > 0$ bond samples with large $Y_{\boldsymbol{J}}$ have more weight. If, on the other hand, we set θ_1 to zero, f_Θ has the shape of a Gaussian of width $2/\theta_2$ centered around θ_3. This means the bias function will increase the weight close to θ_3. With an adequate combination of the parameters in Θ it is possible to create a biased bond distribution with enough weight in regions that lead to the desired values of $Y_{\boldsymbol{J}}$. While this recipe is fairly general, we do not exclude the possibility that for some problems other types of bias functions might work better.

To sample from the biased bond distribution $\widetilde{P}_J$, the Metropolis-Hastings algorithm is used, which in this particular case works as follows. Suppose that we start with a bond sample $\boldsymbol{J}_\mu$ with the corresponding value $Y_{\boldsymbol{J}_\mu}$ of the observable of interest. Now, one generates a candidate bond sample $\boldsymbol{J}'_\mu$ by randomly selecting one or more bonds of $\boldsymbol{J}_\mu$ and assigning to them new coupling values according to the unbiased distribution (2). In other words, a randomly selected bond is set to 1 with probability p and to 0 with probability $1-p$. After computing the observable value for the proposed sample, $Y_{\boldsymbol{J}'_\mu}$, the new bond configuration is accepted with probability

$$A\left(\boldsymbol{J}_\mu \to \boldsymbol{J}'_\mu\right) = \min\left\{1, \frac{f_\Theta\left(Y_{\boldsymbol{J}'_\mu}\right)}{f_\Theta\left(Y_{\boldsymbol{J}_\mu}\right)}\right\}. \tag{10}$$

As a result, the new sample in the Monte Carlo chain $\boldsymbol{J}_\nu$ will be $\boldsymbol{J}_\nu = \boldsymbol{J}'_\mu$ if the proposed sample is accepted, or $\boldsymbol{J}_\nu = \boldsymbol{J}_\mu$ otherwise.

Finally, we establish a connection to the unbiased bond distribution by noticing that

$$\begin{aligned}\widetilde{P}_Y(Y; \Theta) &= \sum_{\boldsymbol{J}} \widetilde{P}_J(\boldsymbol{J}; \Theta)\, \delta[Y_{\boldsymbol{J}} - Y] \\ &= \frac{f_\Theta(Y)}{Z_\Theta} P_Y(Y)\end{aligned}$$

and hence

$$P_Y(Y) = \frac{Z_\Theta}{f_\Theta(Y)} \widetilde{P}_Y(Y; \Theta). \tag{11}$$

If one would like to sample P_Y over a wide range of the support, it is possible to use multiple parameter sets Θ_k, $k = 1, 2, \ldots, K$. After completing the simulations, the biases are corrected by utilizing Eq. (11). In order to achieve this, it is necessary to determine the constants Z_{Θ_k} which can be deduced from the continuity of the

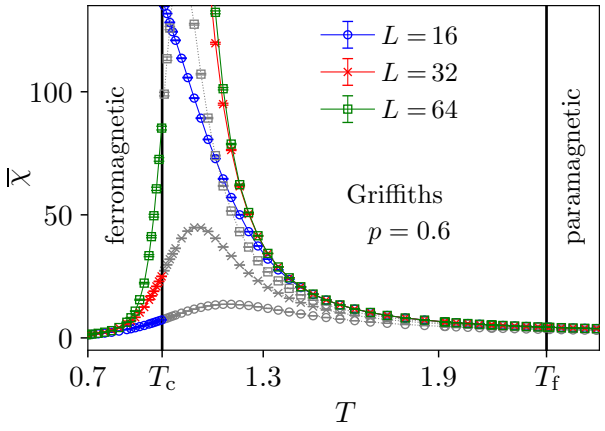

FIG. 4. The mean magnetic susceptibility $\overline{\chi}$ as a function of temperature T for a fraction $p = 0.6$ of ferromagnetic bonds. The values for the different configurations $\boldsymbol{J}$ are computed according to the estimator of Eq. (13). The grey lines are continuations of the low-temperature cluster estimator into the high-temperature phase. These curves exhibit a peak which shifts towards the critical temperature on increasing the system size, similar to other finite-size definitions of χ. The Griffiths phase extends from the critical temperature of the pure ferromagnet $T_f = 2.2691\ldots$ to the corresponding temperature of the diluted system $T_c(0.6) = 0.9541(10)$.

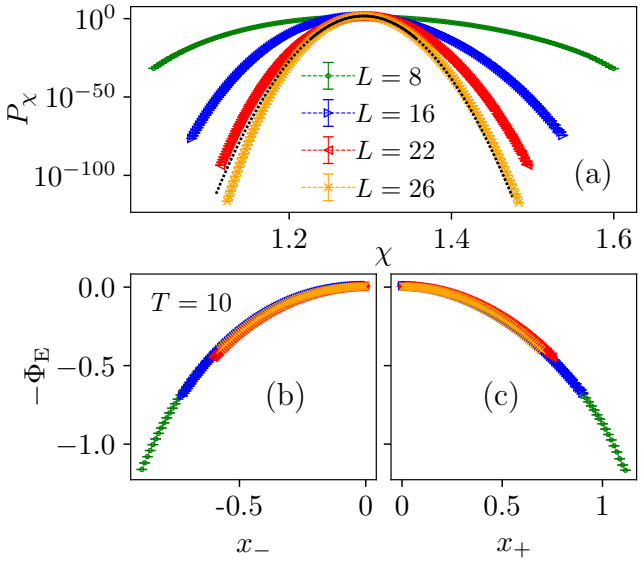

FIG. 5. Histogram of the magnetic susceptibility at temperature $T = 10$, deep inside the paramagnetic phase. (a) Histogram of χ on a logarithmic scale for different system sizes. The full black line on top of the orange curve for $L = 26$ corresponds to a Gaussian fit of type $f(x) = c_1 \exp[-c_2(x - c_3)^2]$ where c_1, c_2 and c_3 are fit parameters, and the dotted black line is an extrapolation of this fit. Close to the mean the fit approximates the data quite well. Panels (b) and (c) depict the empirical rate function as defined in Eq. (16) by using a rescaling of the argument according to Eq. (17). In both cases the data collapse onto a single curve. The mean value $\overline{\chi} = 1.291\,359(22)$ is independent of system size within error bars, as is $\chi_f = 1.5670(23)$.

overall distribution. In other words, in regions where two distributions with parameters Θ_i and Θ_j overlap, their weight should be identical,

$$\frac{Z_{\Theta_i}}{f_{\Theta_i}(Y)} \widetilde{P}_Y\left(Y;\Theta_i\right) = \frac{Z_{\Theta_j}}{f_{\Theta_j}(Y)} \widetilde{P}_Y\left(Y;\Theta_j\right). \tag{12}$$

In case of the unbiased distribution $k = u$ with $\Theta_u = (0,0,0)$ and $\widetilde{P}_Y(Y;\Theta_u) = P_Y(Y)$ we know that $Z_{\Theta_u} = 1$. As a result Z_{Θ_k}, $k = 1, \ldots, K$ can be generated according to Eq. (12) in a successive manner from overlapping distributions starting with $Z_{\Theta_u} = 1$. A useful implementation of this process is described in Ref. [39]. Once the constants Z_{Θ_k} have been fixed, the reweighting according to Eq. (11) is performed and one obtains the final distribution.

To estimate the value of the magnetic susceptibility for a given bond configuration it is necessary to compute an average over multiple thermal samples (since the susceptibility is no "configurational" quantity [40]). To this end, we carry out a thermal Monte Carlo simulation utilizing the Swendsen-Wang cluster algorithm [41]. This method is known to perform well for diluted ferromagnets [42], and it is possible to use improved cluster estimators for the susceptibility [43]. Furthermore, the clusters underlying the algorithm provide an interesting geometrical interpretation of the magnetic susceptibility. To elucidate this context, in the following we hence provide a short exposition of the Swendsen-Wang algorithm as well as the corresponding cluster framework. Starting with a given spin configuration, in the Swendsen-Wang algorithm one *occupies* each bond $J_{\boldsymbol{xy}} > 0$ with probability $p_{\mathrm{FK}}(J_{\boldsymbol{xy}}) = 1 - \exp(-2/T)$ if the two connected spins are parallel, i.e., if $s_{\boldsymbol{x}} s_{\boldsymbol{y}} = 1$, and $p_{\mathrm{FK}}(J_{\boldsymbol{xy}}) = 0$ if $s_{\boldsymbol{x}} s_{\boldsymbol{y}} = -1$. On the contrary, diluted bonds with $J_{\boldsymbol{xy}} = 0$ are never occupied. Two spin sites which are connected by a path of occupied bonds belong to the same cluster. Clusters which are defined in this way are denoted as FKCK (Fortuin-Kasteleyn–Coniglio-Klein) clusters [44]. The smallest possible FKCK cluster contains only a single spin site. After constructing the clusters, each of them is randomly assigned an up or down orientation and the spins in each cluster are flipped accordingly. As a result all spins within each cluster have identical sign but the sign of two spins in different clusters may differ. This generates the next spin configuration of the Monte Carlo process. The Swendsen-Wang algorithm is ergodic and satisfies the detailed balance condition with respect to the Boltzmann distribution [29]. The cluster estimator of the magnetic susceptibility is based on the densities $\hat{\rho}_i$ of the clusters which are defined as their number of sites divided by N. We assume that the indices i are sorted decreasingly by cluster size. For $T \geq T_c$ the estimator is given by the average cluster size of all FKCK clusters [43]. For $T < T_c$ it is necessary to subtract the

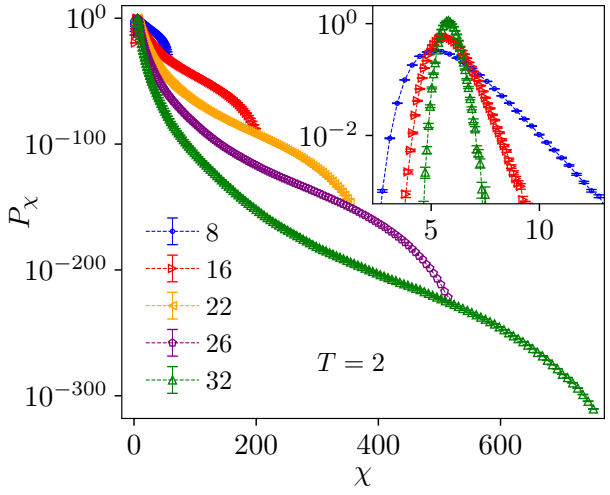

FIG. 6. Histogram of the magnetic susceptibility inside the Griffiths phase at $T = 2$ for multiple system sizes. Within error bars and for $L \geq 16$, the mean is independent of system size and attains the values $\overline{\chi} = 5.8304(11)$. The exponential tail is clearly visible. The inset shows histograms which are obtained by sampling from the unbiased bond distribution, see Eq. (2). For system sizes $L = 8$ (blue circles) $N_J = 10^6$ bond samples are used, for systems size $L = 16$ (red right-pointing triangles) $N_J = 6 \times 10^5$ and for $L = 32$ (green upward-pointing triangles) $N_J = 1.1 \times 10^5$. The data demonstrate that using the standard sampling approach it is only possible to sample a tiny region close to the mean of the distribution.

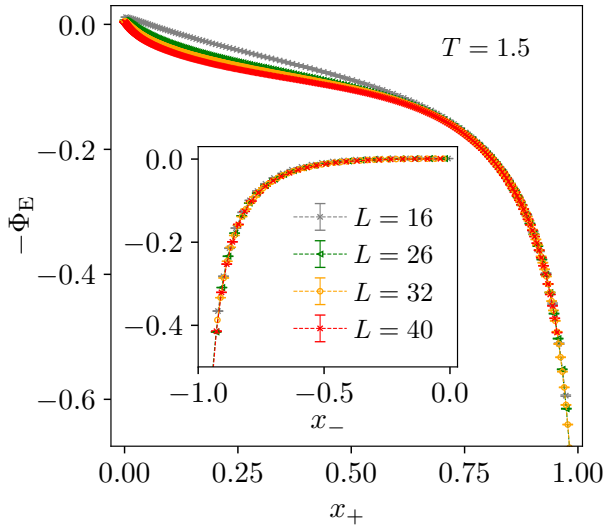

FIG. 7. The empirical rate function at $T = 1.5$ deep inside the Griffiths phase for various system sizes. For $x < 0$ the data collapse well onto a single curve and for $x > 0$ the collapse becomes good for the studied system sizes when x is larger than approximately 0.75. The mean is almost independent of system size with $\overline{\chi} = 16.057(15)$ for $L = 16$ and $\overline{\chi} = 16.173(8)$ for $L = 32$ while χ_f diverges as $\chi_f \sim N$ since $T < T_f$.

square of the density of the infinite cluster [29, 45–47],

$$\chi_{\boldsymbol{J}} = \begin{cases} N \left\langle \sum_{i=1} \hat{\rho}_i^2 \right\rangle_{\mathrm{FK}} & \text{if } T \geq T_c \\ N \left(\left\langle \sum_{i=1} \hat{\rho}_i^2 \right\rangle_{\mathrm{FK}} - \langle \hat{\rho}_1 \rangle_{\mathrm{FK}}^2 \right) & \text{if } T < T_c \end{cases} . \quad (13)$$

The sum is performed over the densities $\hat{\rho}_i$ of all clusters. In the thermodynamic limit and inside the ferromagnetic phase there exists a single infinite cluster whose density $\langle \hat{\rho}_1 \rangle_{\mathrm{FK}}$ is equal to the absolute value of the magnetization per site [2]. In the numerically studied finite-size systems we have taken the cluster of largest size as a proxy for the infinite cluster.

To numerically estimate $\chi_{\boldsymbol{J}}$, we perform a thermal average over N_S cluster configurations. Due to the computational complexity of the problem successive configurations from the Monte Carlo chain are used, such that these individual estimates are correlated. The computational complexity emerges since one has to compute a thermal average each time a new bond sample is proposed. While we need to compute $\chi_{\boldsymbol{J}}$ for each bond update, measurements are only recorded for analysis after each sweep consisting of $2N$ bond updates according to the bond Monte Carlo algorithm, see Eq. (10). Figure 2 shows the sampling of $\chi_{\boldsymbol{J}}$ for systems of size $L = 10$ with $p = 0.6$ and $N_S = 2000$ samples at temperature $T = 2$. The parameters used to generate the data are listed in Table I. As discussed above, $\theta_1 < 0$ leads to a decrease of χ and $\theta_1 > 0$ leads to an increase of $\chi_{\boldsymbol{J}}$ compared to the unbiased case $\Theta_u = (0, 0, 0)$. For $\Theta_3 = (0.9, 0, 0)$ the Monte Carlo chain oscillates between two equilibrium states. The gap between these states increases with system size such that sampling in the intermediate region becomes difficult, and the algorithm is not well suited to study larger systems with $\theta_2 = \theta_3 = 0$ [31]. This problem can be circumvented by using an appropriate combination of non-zero values for θ_2 and θ_3; this is illustrated in Fig. 2. The Figure shows the data of 11 parameter sets for a system of size $L = 10$. For larger systems one has to increase the number of parameter sets to sample the distribution over a wide range of the support such that computations become more and more time-consuming. To generate the histogram for the largest studied system size $L = 128$, see Fig. 13, we used around 320 parameter sets.

To ensure that the Monte Carlo chain is in equilibrium we initialize the lattice with no bonds or all bonds present and wait until both processes oscillate around about the same value, within the fluctuations. Only then the sampling is started. After such sampling is completed, the data are combined into a single histogram by using Eq. (11).

Figure 3 depicts histograms of the distribution of the magnetic susceptibility at system size $L = 16$ with $p = 0.6$ and temperature $T = 2$. As is clearly visi-

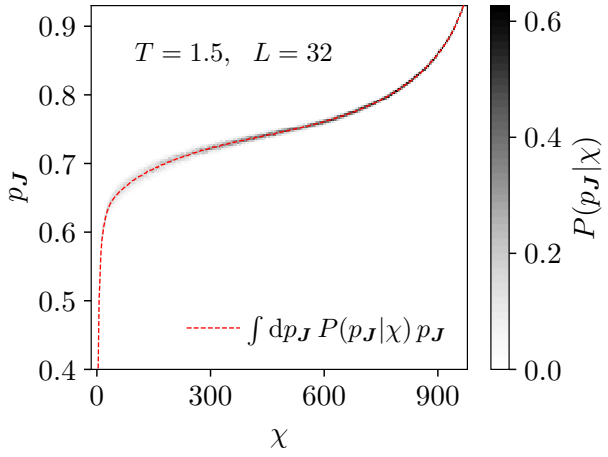

FIG. 8. Connection between the value χ of the magnetic susceptibility and the fraction p_J of ferromagnetic bonds at temperature $T = 1.5$ and system size $L = 32$. The heat map illustrates the probability to measure the fraction of ferromagnetic bonds p_J given the magnetic susceptibility χ, denoted as $P(p_J|\chi)$. The dotted red line corresponds to the conditional mean value of the fraction of ferromagnetic bonds.

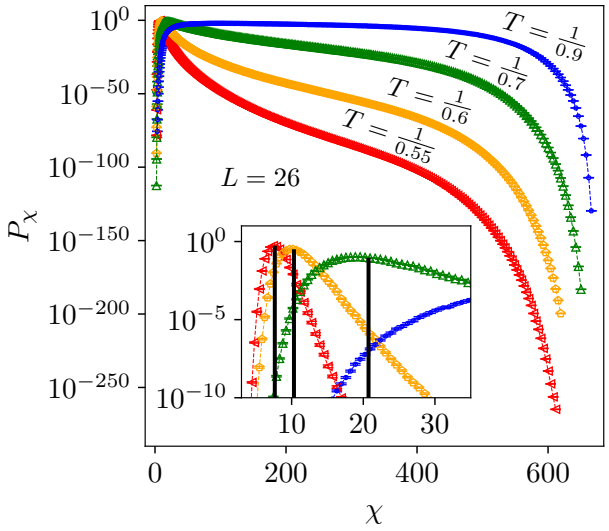

FIG. 9. Histogram of the magnetic susceptibility for different temperatures T in the Griffiths phase. The temperatures reach from the higher temperature Griffiths phase just below T_f at $T = 1/0.55 = 1.\overline{81}$ down to $T = 1/0.9 = 1.\overline{1}$, just above the ferromagnetic transition point at $T_\mathrm{c}(0.6) = 0.9541(10)$. The inset shows the histograms close to the mean. The black vertical lines mark the values of the means.

ble, the distributions depend on the number N_S of spin configurations that are used to estimate χ_J. The histograms are expected to converge to the asymptotic ones for $N_\mathrm{S} \to \infty$. In some cases the convergence can be described by a power law as is demonstrated in the inset of Fig. 3. Because this does not consistently work well for all parts of the distributions for all investigated temperatures, we finally settled on using $N_\mathrm{S} = 2000$ as a trade-off between computational effort and accuracy throughout the rest of this article. The error bars of the distributions are computed by bootstrapping as described in Ref. [48].

IV. RESULTS FOR THE DISORDERED PHASE AND THE CRITICAL POINT

We focus our simulations of the two-dimensional bond-diluted Ising ferromagnet on the case of a fraction of ferromagnetic bonds of $p = 0.6$, which is sufficiently far away both from the pure model as well as from the percolation point. We employ periodic boundary conditions along both axes. For reference, in Fig. 4 we display the temperature dependence of the disorder average of the magnetic susceptibility,

$$\overline{\chi} = [\chi_J]_J \,, \tag{14}$$

estimated according to Eq. (13). The critical temperature of the system is obtained by a finite-size scaling analysis of the wrapping probabilities of the FKCK clusters, resulting in the estimate $T_\mathrm{c}(0.6) = 0.9541(10)$ which is consistent with previous works [34, 37], for details see Appendix A. The Griffiths phase extends from the critical temperature of the pure ferromagnet $T_\mathrm{f} = 2.2691\ldots$ down to $T_\mathrm{c}(0.6) = 0.9541(10)$.

For $T > T_\mathrm{f}$ the distribution of the magnetic susceptibility is expected to be fully concentrated around its mean with a width that decreases by increasing the system size and that ultimately becomes zero in the thermodynamic limit. In order to test these predictions we extracted the distribution of the magnetic susceptibility at $T = 10$ deep inside the paramagnetic phase. Figure 5 shows this distribution for a range of various system sizes. The width of the distribution decreases with system size. The shape of the distribution in the vicinity of the mean can be approximated by a Gaussian.

Further away from the mean the theory of large deviations provides an appropriate toolbox to describe a distribution [49]. A central element of large deviations theory is the rate function Φ that characterizes the probabilities of exponentially rare events. Following this approach, the exponential tail of the distribution of an intensive quantity x which satisfies the so called large-deviation principle can be written as

$$P_x(x; N) = \exp\{-\Phi(x)N + o(N)\} \tag{15}$$

in the limit $N \to \infty$, where $o(N)$ corresponds to the "small o notation". If the large-deviation principle holds, it means that the size dependence of $P_x(x; N)$ on N can be separated from the dependence on x. For finite systems and in case of sufficiently fast convergence the empirical rate function

$$\Phi_\mathrm{E}(x; N) = -\frac{1}{N} \ln\{P_x(x; N)\} \tag{16}$$

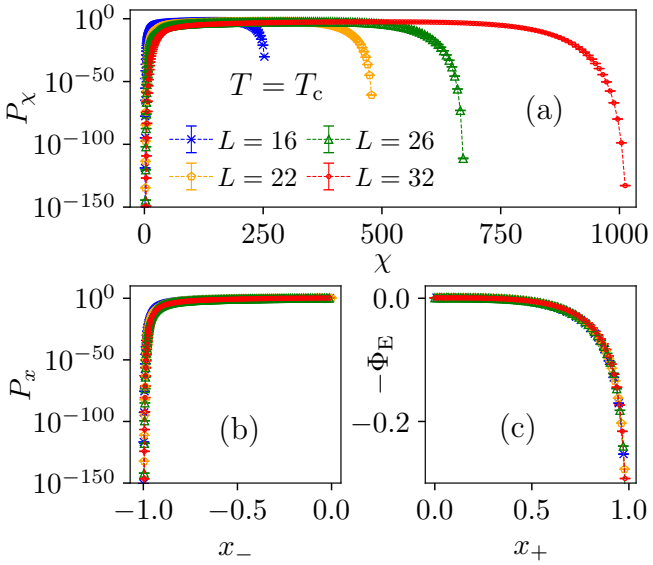

FIG. 10. Histogram of the magnetic susceptibility at the critical temperature. (a) Distribution of χ for multiple system sizes on a logarithmic scale. (b) Collapse of the data left of the mean by a rescaling of the x-axis, demonstrating the lack of self-averaging. (c) Empirical rate function right of the mean.

will provide a good approximation of Φ. The magnetic susceptibility is an extensive quantity. Therefore it is necessary to perform a rescaling to obtain a well defined rate function. While a simple rescaling with N or the mean $\overline{\chi}$ already yields an intensive quantity, we propose the following, somewhat more subtle, rescaling that takes into account the asymmetry of the distribution of χ and uses a different scaling factor to the left and to the right of the mean,

$$x = \begin{cases} x_- = \dfrac{\chi - \overline{\chi}}{\overline{\chi} - 1} & \text{if } \chi < \overline{\chi}, \\ x_+ = \dfrac{\chi - \overline{\chi}}{\chi_\mathrm{f} - \overline{\chi}} & \text{if } \chi \geq \overline{\chi}, \end{cases} \tag{17}$$

which we apply for $T \geq T_c$. If $\chi < \overline{\chi}$ we divide by $\overline{\chi} - 1$ because $\chi = 1$ is the minimum value which the magnetic susceptibility can assume for $T \geq T_c$ as one can see from Eq. (13). When $\chi \geq \overline{\chi}$ we divide by $\chi_\mathrm{f} - \overline{\chi}$ where χ_f corresponds to the magnetic susceptibility of the pure ferromagnet in the high-temperature phase,

$$\chi_\mathrm{f} := N\langle \hat{m}^2 \rangle_S \quad \text{for } p = 1. \tag{18}$$

By doing so we assume that χ_f scales in the same way as the largest relevant values of χ at the same temperature.

Figure 5 shows the empirical rate function of χ at $T = 10$. The data collapse quite well onto a single curve, although some corrections are visible that we expect to diminish further as the system size is increased. Nevertheless, we presume that the empirical rate function gives a good impression of the shape of the rate function for $N \to \infty$, indicating that the assumed large-deviation principle is satisfied.

Next we consider the distribution of the magnetic susceptibility inside the Griffiths phase. Figure 6 illustrates the distribution at temperature $T = 2$ for various system sizes. As in the previous case with $T = 10$, on increasing the system size the distribution contracts around the mean, thus demonstrating the presence of self averaging in the model [7]. Also, the mean $\overline{\chi}$ is essentially independent of system size, but compared to the distribution at $T = 10$ the distribution has acquired a long tail that extends over a wide range of the support.

As discussed above, the analysis of Bray [15] predicts that as a consequence of the Griffiths singularity the tail of the distribution of the magnetic susceptibility extends to infinity. To check this prediction, the rate function is investigated deep inside the Griffiths phase. Figure 7 shows the empirical rate function at $T = 1.5$. Again, the mean is essentially independent of system size. The rescaling according to Eq. (17) leads to a good data collapse on the left side of the mean. On the other hand, to the right of the mean the data collapse becomes better with increasing x_+ such that at $x_+ \approx 0.75$ all curves start to fall on top of each other. Note that since $T < T_\mathrm{f}$, χ_f scales as $\chi_\mathrm{f} \sim N$. As a consequence, the empirical rate function demonstrates that the exponential tail does not become smaller with system size but will reach into infinity for $N \to \infty$. The data are therefore fully consistent with the expected behavior resulting from the Griffiths singularity.

Bray [15] also derived a lower bound for the exponential tail, resulting in the functional form of Eq. (6). Hence, the corresponding rate function is given by $\Phi(x) = Ax$, $x > 0$, see also Appendix B. Qualitatively, the data are consistent with an exponential tail, but the exponent does not seem to be a purely linear function. The rate function is linear if its second derivative is zero. In case of $L = 40$, for instance, the second derivative of the empirical rate function changes its sign in the range of $0.25 \leq x_+ \leq 0.5$ but it is not zero in the whole interval, cf. Fig. 7. If there was an interval where the second derivative was zero and this interval was to increase in size as $N \to \infty$, this would imply a partially linear rate function in agreement with the prediction of Bray. Unfortunately, the data for the relatively small system sizes studied here do not provide a clear indication for such a behavior.

Large values in χ are expected to be linked to compact structures of ferromagnetic bonds with a higher fraction of present bonds [15]. The fraction $p_{\boldsymbol{J}}$ of ferromagnetic bonds for a given bond sample $\boldsymbol{J}$ can be formally expressed as

$$p_{\boldsymbol{J}} = \frac{1}{2N} \sum_{\langle \boldsymbol{x}, \boldsymbol{y} \rangle} J_{\boldsymbol{x}\boldsymbol{y}}. \tag{19}$$

In Fig. 8 we show the correlation between the fraction of ferromagnetic bonds $p_{\boldsymbol{J}}$ and the magnetic susceptibility χ

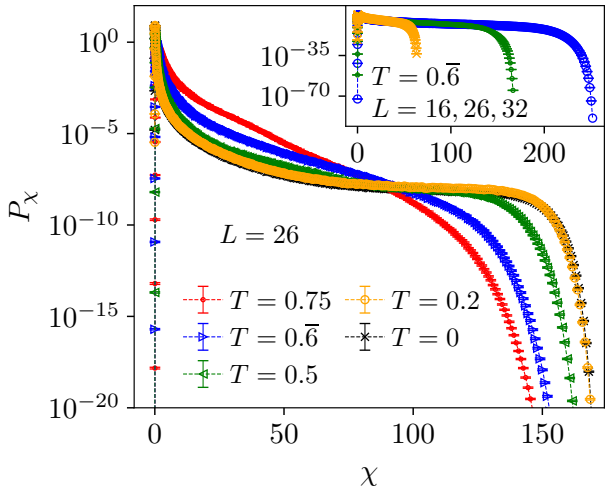

FIG. 11. Histogram of the magnetic susceptibility for different temperatures below the ferromagnetic phase transition at system size $L = 26$. The temperatures reach from $T = 0.75$, which is relatively close to the phase transition, down to the ground state at $T = 0$. The inset shows the magnetic susceptibility at $T = 1/1.5 = 0.\overline{6}$ for three different system sizes $L = 16$, $L = 26$ and $L = 32$. It demonstrates how the tail of the distribution widens rapidly with increasing system size.

by using the conditional probability $P(p_{\boldsymbol{J}}|\chi)$. As one can see, the fraction of ferromagnetic bonds and the value of χ are indeed correlated. Large values of χ are connected to large values of $p_{\boldsymbol{J}}$ and small values of χ to small values of $p_{\boldsymbol{J}}$, respectively. This confirms the predictions.

Another relevant aspect concerns the temperature dependence of the probability distribution of susceptibilities for $T > T_c$. Figure 9 illustrates the distribution for multiple temperatures above T_c. By lowering the temperature the mean of the distribution shifts to larger values. More weight relocates into the tail of the distribution and it becomes flatter. This is in qualitative agreement with the predictions of Bray [15].

Finally, Fig. 10 shows the distribution of χ at the critical temperature. The distribution has a concave shape, it is very flat and covers the whole range of the support from $\chi = 1$ to $\chi_f \sim N$. The mean of the distribution diverges according to $\overline{\chi} \sim L^{\gamma_f/\nu_f}$, where $\gamma_f = 7/4$ and $\nu_f = 1$ are the critical exponents of the pure ferromagnet [9, 10]. To the left of the mean there is no convergence to a rate function. Instead a good data collapse is obtained by only rescaling the x-axis according to $(\chi - \overline{\chi})/\overline{\chi}$, without taking the log of the probabilities and rescaling. The origin of this behavior is the lack of self averaging at criticality in case of the diluted ferromagnet [50, 51]. To the right of the mean the large-deviation principle seems to be satisfied and one obtains a good collapse of the data by using a scaling rule according to Eq. (17).

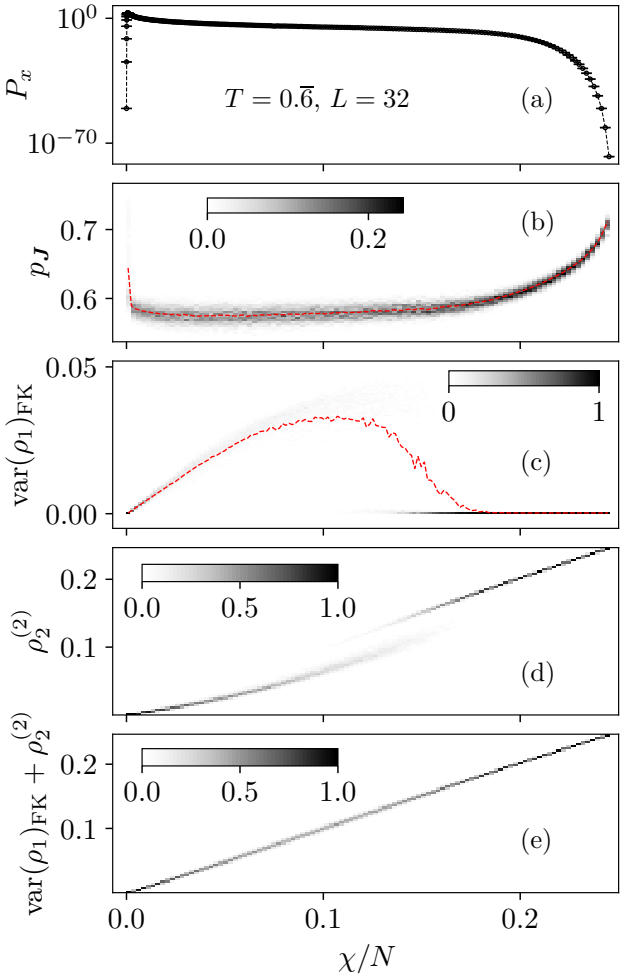

FIG. 12. Histogram of the magnetic susceptibility at $T = 1/1.5 = 0.\overline{6}$ inside the ferromagnetic phase and heat maps of various conditional observables. All plots share the same x-axis which corresponds to the magnetic susceptibility divided by N. (a) Histogram of the magnetic susceptibility. (b) Connection between the fraction of ferromagnetic bonds and the value of the susceptibility expressed through the conditional probability $P(p_{\boldsymbol{J}}|\chi)$. The dotted red line is the conditional mean and shall serve as a guide to the eye. (c) Connection of χ to the variance of the largest FKCK cluster, $P(\mathrm{var}(\rho_1)_{\mathrm{FK}}|\chi)$. (d) Influence of the second moment of the second largest FKCK cluster, $\rho_2^{(2)}$, on χ, i.e., $P(\rho_2^{(2)}|\chi)$. (e) Distribution $P(\mathrm{var}(\rho_1)_{\mathrm{FK}} + \rho_2^{(2)}|\chi)$, demonstrating that $\chi \approx N\left(\mathrm{var}(\rho_1)_{\mathrm{FK}} + \rho_2^{(2)}\right)$.

V. RESULTS FOR THE FERROMAGNETIC PHASE AND AT ZERO TEMPERATURE

In this Section the distribution of the magnetic susceptibility below the ferromagnetic-to-Griffith transition temperature $T_c(p)$ is investigated [52]. Figure 11 shows the distribution of the susceptibility for multiple temperatures inside the ferromagnetic phase. Apart from

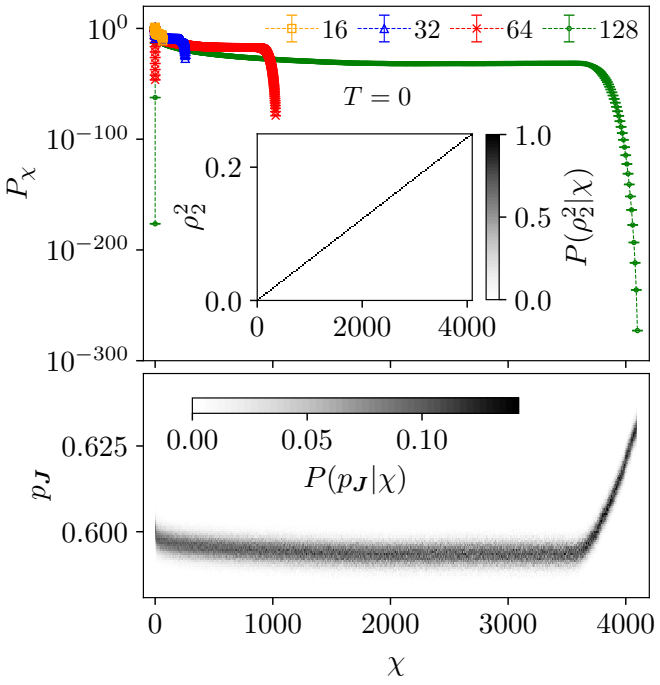

FIG. 13. Histogram of the magnetic susceptibility and connected quantities at $T = 0$. The main plot at the top shows the histogram of the magnetic susceptibility for multiple system sizes. The inset is a heat map which visualizes the conditional probability to obtain a certain density of the second largest cluster ρ_2 given the magnetic susceptibility χ, $P(\rho_2^2|\chi)$. The linear relation between χ and ρ_2^2 is clearly visible. The heat map at the bottom of the figure shares the x-axis with the main plot and illustrates the conditional probability to obtain the fraction of ferromagnetic bonds p_J given the magnetic susceptibility χ, $P(p_J|\chi)$, for system size $L = 128$.

a strong peak close to the mean value there exits an intermediate range where the distribution only decays relatively slowly before it again starts to rapidly fall off. This intermediate range in the tail of the distribution becomes wider and flatter on lowering the temperature such that there exits a pronounced plateau region for $T = 0$. The distribution for $T = 0.2$ is already very similar to that of the ground state behavior found at zero temperature.

In order to unveil the mechanism leading to the large values of the susceptibility in the tail of the distribution inside the ferromagnetic phase, we investigated the correlations of such large susceptibilities to various other observables. Figure 12 shows the histogram of the susceptibility at $T = 0.\overline{6}$ [panel (a)] and the connection to multiple other quantities for system size $L = 32$ [panels (b)-(e)]. It is visible from panel (b) that the local fraction p_J of ferromagnetic bonds is relatively constant over a wider range of the distribution with a value that is slightly smaller than $p = 0.6$. Only for the case where χ is extremely small or large can one observe an increase in p_J [panel (b)]. In the intermediate tail range, the value of the susceptibility is composed of mainly two contributions, the variance of the largest FKCK cluster, $\mathrm{var}(\rho_1)_{\mathrm{FK}} = \langle \hat{\rho}_1^2 \rangle_{\mathrm{FK}} - \langle \hat{\rho}_1 \rangle_{\mathrm{FK}}^2$ [panel (c)], and the second moment of the second largest FKCK cluster, $\rho_2^{(2)} = \langle \hat{\rho}_2^2 \rangle_{\mathrm{FK}}$ [panel (d)], i.e., $\chi \approx N \left(\mathrm{var}(\rho_1)_{\mathrm{FK}} + \rho_2^{(2)} \right)$ [panel (e)], cf. the general form shown in Eq. (13). The contribution of smaller clusters does not seem to be significant.

The contribution of $\mathrm{var}(\rho_1)_{\mathrm{FK}}$ is only relevant relatively close to the mean of the distribution. The slight decrease of p_J in this region is consistent with large values of $\mathrm{var}(\rho_1)_{\mathrm{FK}}$ since the fraction of ferromagnetic bonds which leads to a critical temperature of $T_c(p^*) = 0.\overline{6}$ is roughly $p^* \approx 0.54$ and thus smaller than $p = 0.6$. For the very large values of χ only $\rho_2^{(2)}$ is important. In the region where there is a jump in $\rho_2^{(2)}$, a second large cluster of ferromagnetic bonds forms, which is not connected to the rest of the system, see the details in Appendix C. As will be shown in the following, this phenomenon can also be directly studied in the zero-temperature distribution of χ.

This zero-temperature distribution is of special interest since it is not affected by thermal fluctuations but, instead, it only depends on the bond disorder. Since there are no thermal fluctuations, the magnetic susceptibility for a fixed realization can be computed exactly. Only in this limit are the FKCK clusters identical to the clusters of ferromagnetic bonds since the FKCK occupation probability is one if there exists a ferromagnetic bond and zero otherwise. The cluster sizes are static and the magnetic susceptibility is equal to the average cluster size without the largest cluster. Because it is not necessary to compute thermal averages the computation time decreases significantly and hence that larger system sizes can be studied.

Figure 13 shows the distribution of the magnetic susceptibility at zero temperature for multiple system sizes. Again, it is visible that the tail of the distribution becomes wider on increasing the system size. Note that in this case the large-deviation approach even allows us to sample over the full support of the distribution. The support extends from the minimal possible value $\chi = 0$, when there is only one cluster which contains all spins, to the maximum value $\chi = N/4$, when there are two clusters of equal size which together contain all spins. This is a direct consequence of Eq. (13) if one approaches the infinite cluster by considering the largest cluster of the finite-size systems under consideration. Figure 13 contains a heat map which illustrates the relation between the magnetic susceptibility and the local fraction of ferromagnetic bonds. It shows that the fraction of ferromagnetic bonds remains almost constant over a wide range of the magnetic susceptibility. Only for large values of χ there is a notable increase in the fraction. In comparison to Figure 12, which shows a similar heat map at $T = 1.5$ inside the Griffiths phase, the interval in which p_J varies is much smaller. Instead the density of the second largest cluster ρ_2 is the driving force for the values

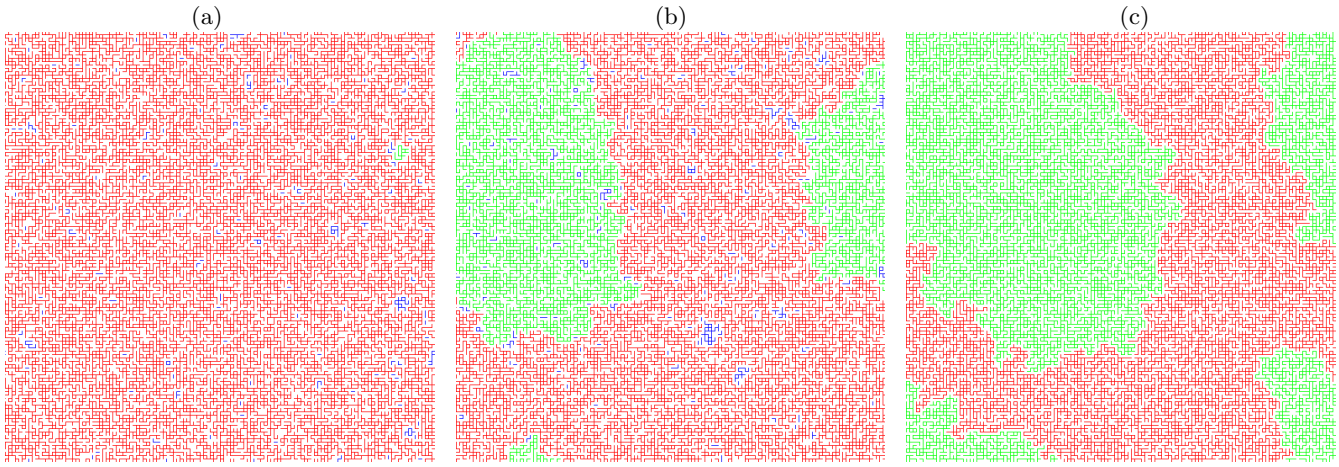

FIG. 14. Three bond samples of size $L = 128$ with different values of $\chi_{\boldsymbol{J}}$ at $T = 0$. Red bonds belong to the largest cluster, green bonds to the second largest cluster, and blue bonds to smaller clusters. Missing bonds are white. Bond sample (a) has susceptibility $\chi_{\boldsymbol{J}} = 0.14233$, which is close to the mean value of the distribution $\overline{\chi} = 0.16016(5)$. Bond sample (b) originates from the intermediate region of the tail of the distribution with $\chi_{\boldsymbol{J}} = 1519.4$ and bond sample (c) comes from the right end of the tail with $\chi_{\boldsymbol{J}} = 4084.0$. The figures illustrate the significance of the second largest cluster for the value of the magnetic susceptibility.

of the magnetic susceptibility. The inset of Fig. 13 shows a heat map of the conditional probability $P(\rho_2^2|\chi)$. It demonstrates that there exists a linear relation between the square of the density of the second largest cluster and the magnetic susceptibility. This central importance of the second largest cluster can also be directly visualized by looking at bond samples with distinct different values of χ as they are shown in Fig. 14. The figure illustrates that for bond samples with a magnetic susceptibility which is close to the mean value the size of the second largest cluster is not important. For bond samples which originate from the plateau region of the distribution, the second largest cluster becomes significant, and for the extreme tail events there are only two clusters left with nearly identical size.

Finally, the behavior of the zero-temperature distribution with system size is studied. The main plot in Fig. 15 shows the logarithm of this distribution divided by L. Note that this is a different type of scaling in comparison to the definition of the empirical rate function given in Eq. (16), where one divides by a factor of $N = L^2$. The scaling with L is a sign of a slower decay behavior of the distribution. The corresponding data collapse is good in the plateau region of the distribution. Because the x-axis is rescaled by a factor of $N/4$, it is possible to conclude that the tail of the distribution will extend to infinity in the thermodynamic limit. The inset of Fig. 15 shows the empirical rate function to the left of the mean. Note that the zero-temperature distribution of the magnetic susceptibility is a special feature of the bond-diluted ferromagnet, i.e., where $J_{\boldsymbol{xy}} = \{0, 1\}$. In the random-bond model with two types of ferromagnetic bonds of different strengths [53], i.e., where $J_{\boldsymbol{xy}} = \{c, 1\}$ with $0 < c < 1$, the distribution of the magnetic susceptibility in the thermodynamic limit will be a delta function at the origin as there is only a single cluster of ferromagnetic bonds which contains all spin sites [54].

Another interesting fact is that the mean of the zero-temperature distribution is non-zero, $\overline{\chi} = 0.16016(5)$. This implies that a field-driven phase transition emerges for very low temperatures since $\partial\overline{m}/\partial h = \overline{\chi}/T$ such that $\partial\overline{m}/\partial h \sim T^{-1}$ for $T \to 0$. The external magnetic field destroys the ground state degeneracy because all spins will align in parallel to the magnetic field.

VI. DISCUSSION

We have studied in depth the distribution of the magnetic susceptibility of the two-dimensional bond-diluted Ising model for a wide range of different temperature covering the paramagnetic, the Griffiths, as well as the ferromagnetic phases down to zero temperature, focusing on a single fraction of ferromagnetic bonds, $p = 0.6$. Due to the adaptation and use of a suitable rare-event sampling algorithm, we are able to follow the distribution for essentially the full range of the support and down to probabilities as small as 10^{-300}. The algorithm is based on the idea proposed in Ref. [30] by one of the present authors to utilize an auxiliary, biased Markov chain in the space of the disorder degrees of freedom, here the space of coupling configurations. We combine this approach with the idea of the multiple Gaussian ensemble of Ref. [33], resulting in an efficient algorithm that performs well even for relatively large systems.

While we cover all phases of the system, our main focus is on the behavior inside the Griffiths phase, which is the thermal region between the ordering transition in the pure ferromagnet and the ferromagnetic transition in its diluted counterpart. It is predicted [15] that in-

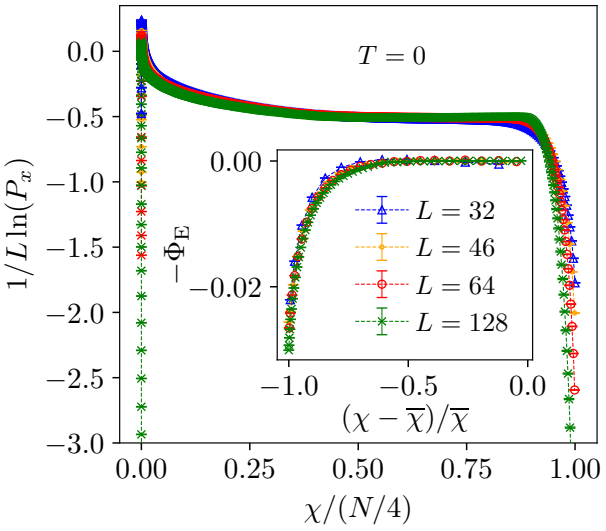

FIG. 15. Scaling of the distribution of the magnetic susceptibility at $T = 0$ for several system sizes. The main plot shows a data collapse of the distribution to the right of the mean. Note that the y-axis is not scaled according to the definition of the empirical rate function in Eq. (16). The chosen scaling gives a good collapse within the plateau region of the distribution. The inset shows the empirical rate function to the left of the mean, $\overline{\chi} = 0.16016(5)$. For large system sizes a good collapse of the data is obtained.

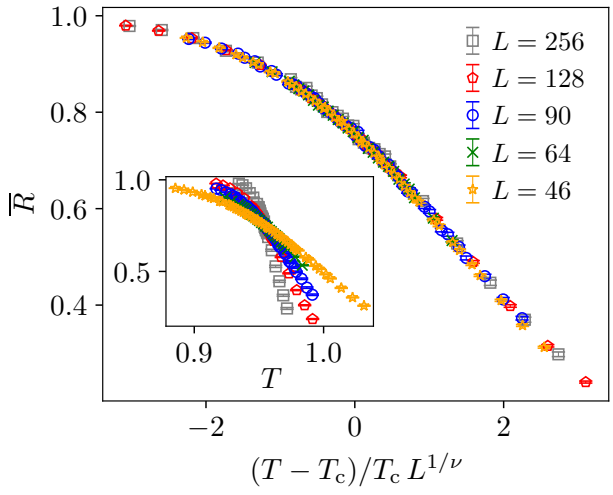

FIG. 16. Finite-size scaling of the wrapping probability of FKCK clusters for $p = 0.6$. The inset shows the original data and the main plot is a data collapse with $T_c = 0.9541(10)$ and $1/\nu = 0.90(14)$. To find the optimal parameters for the collapse we used the tool provided in Ref. [55].

side the Griffiths phase the distribution of the magnetic susceptibility has an exponential tail which extends to infinity, which is a sign of the essential but weak Griffiths singularity. This singularity is caused by arbitrarily large structures of ferromagnetic bonds in which the local fraction of ferromagnetic bonds is higher than the average value. Within these structures the system is effectively in a ferromagnetic state such that a change of the orientation of the spins can lead to large values of the magnetic susceptibility. By sampling the distribution of the magnetic susceptibility over a wide range of the support it is possible to uncover the exponential tail which emerges inside the Griffiths phase. The connection between the sample fraction of bonds and the size of the magnetic susceptibility is verified numerically.

The distribution of the magnetic susceptibility is also studied directly at the critical temperature and inside the ferromagnetic phase. At the critical temperature a lack of self-averaging is observed to the left of the distribution mean, i.e., for small values of χ [50, 51]. Inside the ferromagnetic phase the distribution of the magnetic susceptibility exhibits an exponential tail similar to that of the Griffiths phase. The tail becomes wider with increasing system size and it is expected to extend to infinity in the thermodynamic limit. It is found that the driving force behind large values of the magnetic susceptibility in the ordered phase is a combination of the variance of the largest FKCK cluster and the size of the second largest cluster. At zero-temperature the second term, the size of the largest cluster of ferromagnetic bonds, is the only contribution to the large susceptibility observed.

The Griffith phase is not particular to the diluted ferromagnet, but it can also be observed in other disordered systems, and we hope that the present work will motivate similar studies of related phenomena in related models. Of particular interest could be the case of the two-dimensional Ising spin glass [20]. This model exhibits frustrated interactions and does not have a ferromagnetic phase transition. Thus it would be interesting to see how the distribution of the magnetic susceptibility is impacted by these differences. Furthermore, we expect that similar effects of broad distributions will also be visible in observables other than the magnetic susceptibility. For the diluted ferromagnet studied here, for instance, the distribution of the specific heat would be of special significance since the specific heat describes the fluctuations of the internal energy that becomes singular at the ferromagnetic phase transition just as the magnetic fluctuations represented in the susceptibility. Finally, it would me most intriguing to apply the rare-event sampling techniques showcased here also for the case of the Griffiths singularities observed in quantum systems [21–27].

ACKNOWLEDGMENTS

The authors thank F. Hucht for interesting discussions.

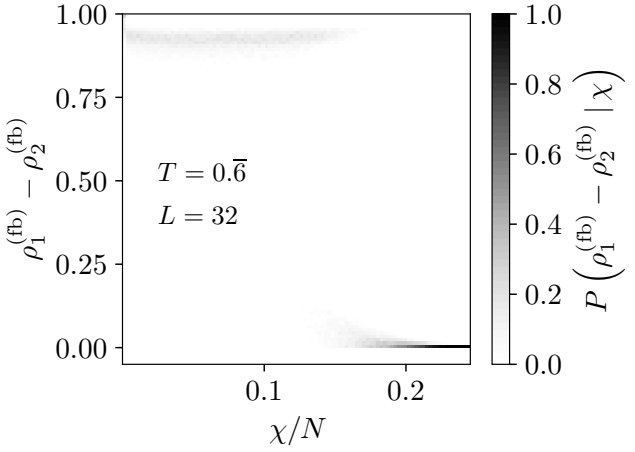

FIG. 17. Difference in density of the two largest clusters of ferromagnetic bonds for a given value of χ at temperature $T = 0.\overline{6}$ and system size $L = 32$.

Appendix A: Estimation of the critical temperature

To determine the critical temperature for $p = 0.6$, we performed a finite-size scaling analysis of the wrapping probabilities $\overline{R}(T)$ of the FKCK clusters. For our purposes, we define the wrapping probability as the probability that there exists a connected path of occupied bonds which wraps around the boundaries along the x-axis, the y-axis or in both directions. Close to the percolation threshold finite-size scaling implies that $\overline{R}(T)$ should behave as [56]

$$\overline{R}(T, L) = f_{\overline{R}}\left\{(T - T_{\mathrm{c}})/T_{\mathrm{c}} L^{1/\nu}\right\}, \tag{A1}$$

where $f_{\overline{R}}$ is a scaling function. Figure 16 shows the wrapping probability as a function of temperature for several system sizes. The number of bond samples used to perform the average over disorder ranges from $N_J = 11\,000$ for the smallest system size $L = 46$ to $N_J = 1100$ for the largest system size $L = 256$. A collapse of the data according to Eq. (A1) leads to a critical temperature of $T_{\mathrm{c}} = 0.9541(10)$ and the critical exponent $1/\nu = 0.90(14)$. The reason for the deviation from the value of the pure ferromagnet, where $\nu_{\mathrm{f}} = 1$, are most likely finite-size scaling corrections that are not accounted for in the collapse approach. The estimate of the critical temperature is consistent with previous results [34, 37].

Appendix B: Exponential tail according to Bray

In Ref. [15] Bray derived a functional form for the exponential tail of the distribution of the inverse magnetic susceptibility χ^{-1} over the bond disorder inside the Griffiths phase. In the limit $\chi^{-1} \to 0$ he arrives at the following form for the distribution:

$$P_{\chi^{-1}}(\chi^{-1}) \sim \exp\left(-\frac{A}{\chi^{-1}}\right),$$

where A is a temperature dependent positive constant. By performing a change of variables one obtains the tail as a function of χ,

$$P_{\chi}(\chi) \sim \chi^{-2} \exp(-A\,\chi).$$

Below T_{f} and outside of the critical region, we have $\chi_{\mathrm{f}} \sim N$ such that one can define the intensive quantity $x = \chi/N$ which gives $P_x(x; N) = \exp(-AxN - 2\ln(x) - \ln(N))$. The corresponding rate function then is given by

$$\lim_{N\to\infty} -\frac{1}{N} \ln\{P_x(x; N)\} = Ax. \tag{B1}$$

Appendix C: Ferromagnetic bond clusters

Ferromagnetic bond clusters are defined by lattice sites which are connected by a path of ferromagnetic bonds, i.e., they correspond to the FKCK clusters at $T = 0$. The density of a ferromagnetic bond cluster is given by the number of lattice sites which it contains divided by N. Figure 17 shows the difference in density of the two largest clusters of ferromagnetic bonds, $\rho_1^{(\mathrm{fb})} - \rho_2^{(\mathrm{fb})}$. For $\chi/N \geq 0.2$ the second largest cluster has almost the same size as the largest cluster, since $\rho_1^{(\mathrm{fb})} - \rho_2^{(\mathrm{fb})} \approx 0$. This demonstrates that the second largest cluster of ferromagnetic bonds leads to the very large values of χ inside the ferromagnetic phase at zero and positive temperatures.

[1] S. G. Brush, Rev. Mod. Phys. **39**, 883 (1967).
[2] A. Coniglio and A. Fierro, "Correlated percolation," in *Complex Media and Percolation Theory*, edited by M. Sahimi and A. G. Hunt (Springer, New York, 2021) p. 61.
[3] A. J. Page and R. P. Sear, Phys. Rev. Lett. **97**, 065701 (2006).
[4] A. Grabowski and R. Kosiński, Physica A **361**, 651 (2006).

[5] J. P. Sethna, K. A. Dahmen, and C. R. Myers, Nature **410**, 242 (2001).

[6] D. L. Stein and C. M. Newman, *Spin Glasses and Complexity* (Princeton University Press, Princeton, 2013).

[7] H. Nishimori and G. Ortiz, "Random systems," in *Elements of Phase Transitions and Critical Phenomena* (Oxford University Press, Oxford, 2011) p. 178.

[8] A. B. Harris, J. Phys. C **7**, 1671 (1974).

[9] I. A. Hadjiagapiou, Physica A **390**, 1279 (2011).

[10] J.-S. Wang, W. Selke, V. Dotsenko, and V. Andreichenko, Physica A **164**, 221 (1990).

[11] V. Andreichenko, V. Dotsenko, W. Selke, and J.-S. Wang, Nucl. Phys. B **344**, 531 (1990).

[12] H. Ikeda, M. Suzuki, and M. T. Hutchings, J. Phys. Soc. Jpn. **46**, 1153 (1979).

[13] I. B. Ferreira, A. R. King, V. Jaccarino, J. L. Cardy, and H. J. Guggenheim, Phys. Rev. B **28**, 5192 (1983).

[14] R. B. Griffiths, Phys. Rev. Lett. **23**, 17 (1969).

[15] A. J. Bray, Phys. Rev. Lett. **59**, 586 (1987).

[16] A. J. Bray and M. A. Moore, J. Phys. C **15**, L765 (1982).

[17] S. Colborne and A. Bray, J. of Phys. A **22**, 2505 (1989).

[18] C. Heng, Y. Song-Liu, S. Jing-Lin, J. Xiu-Lin, L. Pai, W. Yong-Qiang, and L. Li, Chin. Phys. Lett. **23**, 1176 (2006).

[19] A. Bray and D. Huifang, Phys. Rev. B **40**, 6980 (1989).

[20] Y. Matsuda, H. Nishimori, and K. Hukushima, J. Phys. A **41**, 324012 (2008).

[21] T. Vojta, Low Temp. Phys. **161**, 299 (2010).

[22] D. S. Fisher, Phys. Rev. Lett. **69**, 534 (1992).

[23] D. S. Fisher, Phys. Rev. B **51**, 6411 (1995).

[24] A. P. Young and H. Rieger, Phys. Rev. B **53**, 8486 (1996).

[25] C. Pich, A. P. Young, H. Rieger, and N. Kawashima, Phys. Rev. Lett. **81**, 5916 (1998).

[26] R. Wang, A. Gebretsadik, S. Ubaid-Kassis, A. Schroeder, T. Vojta, P. J. Baker, F. L. Pratt, S. J. Blundell, T. Lancaster, I. Franke, J. S. Möller, and K. Page, Phys. Rev. Lett. **118**, 267202 (2017).

[27] K. Nishimura, H. Nishimori, and H. G. Katzgraber, Phys. Rev. A **102**, 042403 (2020).

[28] A. K. Hartmann, *Big Practical Guide to Computer Simulations* (World Scientific, Singapore, 2015).

[29] M. E. Newman and G. T. Barkema, *Monte Carlo methods in statistical physics* (Oxford University Press, Oxford, 1999).

[30] A. K. Hartmann, Phys. Rev. E **65**, 056102 (2002).

[31] A. K. Hartmann, Eur. Phys. J. B **84**, 627 (2011).

[32] K. Hukushima and Y. Iba, J. Phys. Conf. Ser. **95**, 012005 (2008).

[33] T. Neuhaus and J. S. Hager, Phys. Rev. E **74**, 036702 (2006).

[34] M. Ohzeki, Phys. Rev. E **79**, 021129 (2009).

[35] Note that below the ferromagnetic phase transition the symmetry is broken such that there are two Gibbs states, one with positive and one with negative magnetization. To obtain the correct value for the magnetization, the average has to be restricted to one of the Gibbs states. In numerical simulations, however, there is usually no symmetry breaking and thus one often uses the absolute value of the magnetization as an estimator for the magnetization or, alternatively, the largest FKCK cluster, see Sec. III.

[36] H. Nishimori, J. Phys. C **12**, L905 (1979).

[37] W. Zhong, G. T. Barkema, and D. Panja, Phys. Rev. E **102**, 022132 (2020).

[38] Note that in most cases we used $Y_{\boldsymbol{J}} = \sqrt{N\chi_{\boldsymbol{J}}}$ instead of $\chi_{\boldsymbol{J}}$ since this quantity is found to be easier to sample. The distribution of $\chi_{\boldsymbol{J}}$ can then be obtained by a change of variables.

[39] H. Schawe, *Large Deviations of Convex Hulls of Random Walks and Other Stochastic Models*, dissertation, Carl von Ossietzky Universität Oldenburg, Oldenburg (2019).

[40] P. L. Ebert, D. Gessert, and M. Weigel, Phys. Rev. E **106**, 045303 (2022).

[41] R. H. Swendsen and J. S. Wang, Phys. Rev. Lett. **58**, 86 (1987).

[42] A. H. Kole, G. T. Barkema, and L. Fritz, Phys. Rev. E **105**, 015313 (2022).

[43] U. Wolff, Phys. Lett. B **228**, 379 (1989).

[44] The FKCK clusters are also called FK clusters or CK droplets due to their historical origin [2], see also Ref. [57].

[45] K. Binder and D. W. Heermann, "Some important recent developments of the Monte Carlo methodology," in *Monte Carlo Simulation in Statistical Physics: An Introduction* (Springer Berlin Heidelberg, Berlin, Heidelberg, 2010) p. 111.

[46] J. Roussenq, A. Coniglio, and D. Stauffer, Journal de Physique Lettres **43**, 703 (1982).

[47] M. Weigel, W. Janke, and C. K. Hu, Phys. Rev. E **65**, 036109 (2002).

[48] A. P. Young, *Everything You Wanted to Know About Data Analysis and Fitting but Were Afraid to Ask* (Springer, Cham, 2015).

[49] H. Touchette, Phys. Rep. **478** (2009).

[50] S. Wiseman and E. Domany, Phys. Rev. E **52**, 3469 (1995).

[51] S. Wiseman and E. Domany, Phys. Rev. Lett. **81** (1998).

[52] As a technical detail we want to mention that for the plots in Fig. 11, Fig. 12 and Fig. 17 we have used the common estimator $\chi_{\boldsymbol{J}} = N(< \hat{m}^2 >_S - < |\hat{m}| >_S^2)$ to compute the magnetic susceptibility since this worked better for sampling at larger system sizes. The results, however, are fully consistent with those of the cluster estimator of Eq. (13) for $T < T_c$.

[53] R. Fisch, J. Stat. Phys. **18**, 111 (1978).

[54] In case of the random ferromagnet with $J_{\boldsymbol{xy}} = \{c, 1\}$ and $0 < c \leq 1$ the variance of the largest FKCK cluster might lead to a tail in the distribution of the magnetic susceptibility inside the ferromagnetic phase above zero temperature, but whether this is indeed the case should be investigated in future studies.

[55] O. Melchert, "autoScale.py - a program for automatic finite-size scaling analyses: a user's guide," (2009), arXiv:0910.5403.

[56] D. Stauffer and A. Aharony, *Introduction to Percolation Theory*, 2nd ed. (Taylor & Francis, London, 1994).

[57] L. Münster and M. Weigel, Phys. Rev. E **107**, 054103 (2023).